To the Graduate Council:

I am submitting herewith a thesis written by Jeffrey A. Evans entitled "Analysis of Luminosity Temperature Measurements of Coal-Fired MHD Plasmas." I have examined the final copy of this thesis for form and content and recommend that it be accepted in partial fulfillment of the requirements for the degree of Master of Science, with a major in Engineering Science.

Trevor V. Giel Jr.
T. V. Giel, Jr., Major Professor

We have read this thesis
and recommend its acceptance:

John E. Caruthers

Roy J. Schulz

Accepted for the Council:

C. W. Minkel
The Graduate School

ANALYSIS OF LUMINOSITY TEMPERATURE MEASUREMENTS
OF COAL-FIRED MHD PLASMAS

A Thesis
Presented for the
Master of Science
Degree
The University of Tennessee

Jeffrey A. Evans

December 1984

ACKNOWLEDGMENTS

The author wishes to thank the members of his thesis committee, Dr. Tom Giel, Jr., Dr. Roy Schulz, and Dr. John Caruthers for their guidance and assistance. Recognition is also given to Mr. Brad Winkleman for his efforts in this respect. Appreciation is also expressed to Madge Gibson for her help in typing portions of this thesis.

A special note of thanks to the author's wife, Marissa, for her endless patience, suggestions, and support. This thesis is dedicated to the author's daughter, Victoria Maria.

ABSTRACT

An optically based temperature measurement technique known as the luminosity probe system was studied and analyzed to determine uncertainty levels in temperatures measured with the system. The system is currently used to determine relative temperatures at the United States Department of Energy's Coal Fired Flow Facility (CFFF) located adjacent to the University of Tennessee Space Institute (UTSI), Tullahoma, Tennessee. The CFFF is an experimental, coal-fired, Magnetohydrodynamics (MHD) power generation development facility.

The uncertainty analysis separates uncertainties into precision and bias errors. Uncertainties in both the luminosity probe temperature determination and measurement spatial resolution are considered. For the temperature determination uncertainties, bias errors are considered to be negligable and only precision errors are evaluated. However, for the spatial resolution uncertainties it is shown that bias errors can be significant. The causes of spatial resolution bias are addressed, resulting in a new probe design to eliminate internal reflection. Bias uncertainties can be eliminated by careful installation of the new probe design.

The luminosity probe response equation, which is based on Planck's radiation law, is expanded into a truncated Taylor series form. This form is then used to derive theoretical estimates of calibration and measured parameter uncertainties, and their effect on the derived temperature. Values for the precision uncertainties in the measured temperature are obtained from test conditions, and their

effects are evaluated using the truncated Taylor series form to determine the precision uncertainty in the temperature.

The major result of this investigation is an improved optical emission temperature measurement system based on luminosity, that is well suited to making relative temperature measurements in coal fired MHD plasmas. For such plasmas, the theoretical uncertainty in the measured temperature is about ±91 K or ±3.6% for a temperature of 2600K which was the nominal value used. It is recommended that further studies be made to determine this uncertainty more accurately and also recommended that care be taken in implementing the luminosity probes to avoid bias uncertainties.

TABLE OF CONTENTS

SECTION PAGE

LIST OF FIGURES

FIGURE PAGE

1.0 INTRODUCTION

1.1 Application of MHD to Power Generation

In recent years attention has been focused on the finite extent of our fossil energy sources. This attention has resulted in increasing concern over the depletion of the most readily available fossil energy sources. As a result a worldwide research effort has been launched to both improve the utilization of alternate resources and also increase the utilization efficiency of current energy sources. At the same time there has been greater emphasis on reducing the environmental impact of our manufacturing processes, including the process of energy production. These concerns have led to research on coal fired Magnetohydrodynamics (MHD). MHD is intended as a topping cycle for conventional coal fired electric power generation plants and theoretically should provide significant energy conversion efficiency. With an MHD topping cycle, an overall plant efficiency of near sixty percent can be reached as opposed to a maximum of about forty percent for conventional plants. The MHD process also provides a potential process for greatly reducing sulphur compound emissions from the plant exhaust stack even if the plant burns high sulfur coal. Thus MHD technology opens the way for utilizing a resource that the United States has in abundance with minimal environmental impact.

Conventional electrical generators are driven by steam turbines powered by steam produced from burning coal in boilers. The electrical generators operate by rotating coils of conducting wire within a fixed magnetic field, which generates electricity according to

Faraday's law. This law states that when a conductor is moved through a magnetic field an electrical current is produced in the conductor. In an MHD generator, the coal combustion products form an electrically conducting plasma which is used to generate electrical current by flowing the gaseous plasma through a fixed magnetic field perpendicular to a flow duct called an MHD channel. The MHD channel has electrically conducting walls to extract the electrical current produced as the plasma cuts through the magnetic field lines. The gases, which are very hot as they leave the MHD channel, are used to generate steam in a conventional manner in a downstream plant.

A conventional coal fired power plant operates at a maximum temperature of about 1500 degrees Kelvin. The MHD plasma gases that leave the channel are somewhat hotter than this, so that some cooling of these exhaust gases may have to be done. Also, it would be desirable to remove the particulate species that result from coal combustion, to avoid fouling problems in the downstream plant. Finally, for the coal fired MHD plasma to be conducting, an alkali seed material is added. This seed must be recovered if the MHD process is to be a commercial success.

1.2 The MHD Plasma

The MHD plasma or combustion gas must have a conductivity on the order of ten siemens. To obtain this degree of conductivity without seed requires a combustion gas temperature on the order of 9000 degrees Kelvin, which is not attainable from a coal-air or coal-oxygen mixture. Thus an easily thermally ionizable seed material, potassium carbonate, is added to the coal. The potassium seed ionizes significantly at coal-air or coal-oxygen combustion temperatures of about 2900 degrees Kelvin. The conductivity of the gas is increased to levels sufficient to create a conductive plasma and make the coal fired MHD process feasible.

At typical coal-air or coal-oxygen combustion temperatures, the potassium seeded plasma conductivity is very sensitive to the plasma temperature, dropping rapidly at temperatures below 2650 K. The plasma conductivity is defined as

$$\sigma = e\, n_e\, \mu_e \quad , \tag{1}$$

where e is the electron charge, n_e is the electron concentration, and μ_e is the electron mobility. The elecron mobility can be derived from collision cross section data based on the specific composition of the gas. The electron concentration and hence the conductivity is exponentially dependent on gas temperature through Saha's relation, given by

$$\frac{n_e^{\,2}}{n_K} = (2.43 \text{ X } 10^{21})\ T^{3/2} \exp(-\frac{\varepsilon_i}{KT}) \quad , \tag{2}$$

where n_K is the potassium atom concentration, T is the temperature, k is Boltzmann's constant (1.388×10^{-23} J/K), ne is the electron concentration as before and ε_i is the potassium ionization potential (4.32 eV). If the temperature in equation 2 is increased from 2650 K to 2900 K, approximately a 10% increase, $n_e^{\,2}/n_k$ would change by a factor of 10, or 100%. Assuming the electron mobility is fairly constant, the conductivity will vary directly with n_e^2/n_k. Thus the relation of conductivity to temperature follows.

1.3 The Need for Plasma Diagnostic Tools

In the course of research into MHD processes it has been discovered that the power output of an MHD generator is also strongly correlated to the spatial uniformity of the conductivity of the plasma [1].

When the temperature profile across the flow is uniform or flat, the plasma conductivity is also uniform if the seed material has been well distributed. If the seed material distribution is not uniform, then the plasma conductivity will not be uniform even if the plasma temperature is uniform. Thus, both uniform temperatures and uniform seed concentrations are required for uniform plasma conductivity. It would be useful to be able to measure the uniformity of the conductivity or the temperature of an MHD plasma for gas diagnostic purposes. Techniques have been developed for measuring plasma temperature and conductivity, but those for measuring the uniformity of the plasma temperature are more developed than those for measuring the uniformity of the conductivity. Unfortunately, standard intrusive temperature measurement devices, such as thermocouples and resistance thermometers, are not adequate for measuring plasma temperatures because the temperatures are well above the useful thermocouple range and sometimes their melting point. Also, the coal fired plasma contains high particulate concentrations, which will erode uncooled probes and condense on cooled probes. Fortunately, it is possible to measure temperatures using certain optically based, nonintrusive systems.

1.4 Current Optically Based Gas Diagnostic Systems

There are several nonintrusive optical systems that can be used to measure gas temperatures. Those of the widest application are Coherent Anti-Stokes Raman Spectroscopy (CARS), spontaneous Raman spectroscopy, laser fluoresence, line reversal, and optical emission measurement or pyrometry.

1.4.1 CARS. The CARS technique mixes two laser sources of frequency ω_1 (the pump frequency) and ω_2 (the Stokes beam) to generate an intense coherent beam at $\omega_3 = 2\omega_1 - \omega_2$ (the Anti-Stokes frequency) when the frequency difference, $\omega_1 - \omega_2$ is tuned to a Raman active molecular vibrational resonance. The intense coherent beam created is actually a laser beam with the gas species being studied the active media. The N_2 molecule is most commonly used as the subject molecule. The two laser beams must be properly aligned so that the three wave mixing process is properly phased. The advantage in using a CARS technique is the relatively strong signal caused by the intense coherent beam, providing the capability of collecting all the signal while optically limiting the background radiation collected. Unfortunately, a CARS system requires very complex and costly equipment to ensure correct alignment and to process the signal into measured parameters. It requires opposed optical ports which is impractical in the system application of interest to the present study.

1.4.2 Spontaneous Raman. Spontaneous Raman spectroscopy has been widely used for combustion diagnostics in clean flames. In spontaneous Raman systems, a single visible wavelength laser is focused on a spot in the gas and gas molecule species scatter light at decreased (Stokes) or increased (anti-Stokes) frequencies. The scattered light from the gas species is collected and its frequency distribution is analyzed to determine the temperature of the molecules which cause the frequency shift. Because of the weak scattered signal found in Raman spectroscopy, it is impractical in particle laden flows or other flows with strong background emissions, such as those found in coal fired MHD flows. It is therefore impossible to use this system in the system application of interest here due to its inherent limitations.

1.4.3 Laser fluorescence. Laser fluorescence is another method that is used for temperature measurement and is one that has been used to obtain relative temperature measurements in MHD flows [2]. This technique uses a laser which is frequency tuned for resonance with the frequency of an absorption line of a specific molecule species. Relative temperatures are found from the resulting fluorescence levels. Data interpretation is complicated by collisional quenching processes which tend to reduce the amount of fluorescence. Laser fluorescence also requires multiple ports and would be very difficult to use in the present system application, i.e. at the nozzle of the CFFF flowtrain

1.4.4 Line reversal. The line reversal technique is based on a comparison of radiation emitted by the plasma alone and by the plasma when it is transilluminated by a reference source. When the brightness temperature of the source is known, comparison of the two signals yields a wavelength specific emissivity. In a modified line reversal technique, when the radiation emitted from the plasma is known and a wavelength specific emissivity is known, wavelength specific temperatures can be derived. This method has been applied and works well for determining plasma temperatures at certain points along the CFFF flowtrain [3]. However, it cannot be implemented at the CFFF nozzle because opposing optical ports cannot be provided in the nozzle.

1.4.5 Optical emission measurement. Optical emission measurement is the simplest and least expensive method of determining relative temperatures. It measures the radiation emitted by the plasma and, assuming a value for the emissivity, determines a temperature. Furthermore, if the emissivity at all measurement points is the same, or is constant with time at one measurement point, relative temperatures can be obtained even if the actual value of the emissivity is unknown. Of course, the emissivities and temperatures are wavelength specific. This system's primary disadvantage is the assumption of constant emissivity, but its advantage is that it uses a single optical port. Thus, this technique may be applied at the nozzle of the CFFF flow train. In fact, the relatively small linear dimensions of the nozzle throat is an asset for the application of the optical emission measurement system. The other advantages of the optical emission technique are that it requires minimal geometric intrusion for optical port access and purging of optical ports. For these reasons this technique was chosen to determine relative temperatures in the nozzle.

The optical emission measurement technique applied at UTSI is basically single wavelength pyrometry. It looks at a bright gas emission line, isolated by a bandpass filter, so that the measurement is of the gas temperature rather than the opposite wall temperature. It uses a small optical port (approximately 1/3 cm in diameter) which in the CFFF flowtrain is purged by nitrogen gas to prevent blockage by coal combustion slag. The system uses an optical probe configuration to collimate the detected light, attain spatial resolution, and ensure proper filter function. As mentioned before, this system provides a temperature measurement based on an assumed emissivity which is itself temperature dependent. Hence it represents a problem of "one equation and two unknowns." Therefore in its application it turns out that the resultant temperatures it provides are "relative." Several probes are situated laterally across the flow so that, if the emissivity can be assumed constant at all probe locations, temperature profiles can be determined.

1.5 Objectives of the Current Research

1.5.1 Purpose of the research. The purpose of this study is to estimate realistic measurement uncertainties in the optical emission (luminosity) temperature measurement system and show how these uncertainties affect the measured temperature profiles, or temporal fluctuation measurements. This uncertainty analysis is composed of two parts. The first part is an attempt to quantify the expected average variation between repeated measurements, called the estimated precision index of the measurement. The precision index is the estimated standard deviation of the random error incurred in repeated measurements. The second part of the uncertainty analysis of the measurement error is an attempt to quantify the bias error. Bias error is the systematic, invariant error defined as the difference between the average of the measurements and the true nominal value of the measurements. The measurement uncertainty, U, is a combination of the bias error, B, and the precision index, S, given mathematically by [4]

$$U = \pm(2S + B) \tag{3}$$

Thus, the purpose of the present research program is to quantify U for the optical emission luminosity temperature measurement system implemented at UTSI in the nozzle of the CFFF MHD flow train.

1.5.2 Uncertainty in terms of bias and precision indices for the present research. The factor of 2 as a multiplier for the precision index, S, is an estimate of the number of standard deviations that when added or subtracted from the true value will include 95% of all measurement values. The value of 2 is used as a compromise [4] between the Student's "t" distribution value of 2.04 for 30 measurements and the Gaussian distribution value of 1.96 for an infinite sampling of measurements. No multiplier is used for the bias since the bias is a nonvarying systematic error, not the standard deviation of an error probability distribution.

Precision indices for various measured parameters can generally be determined as the standard deviation of a number of repeated measurements. Bias, however, is not so easily determined. Known biases, if they are significant, are generally eliminated or corrected for by equipment or system calibration. Large known biases that are not correctable can be taken into account in the data reduction procedures. However, small, unknown biases are difficult to estimate, requiring special calibration procedures and techniques, and operator subjective judgement. In the application of the optical emission technique discussed in this study, special calibrations (such as comparison with ancillary systems for the same gas conditions measured at the nozzle throat) are not feasible. Also, only comparative temperature measurements are obtained with the optical temperature measurement. Therefore the bias of the system cannot be determined in this application. Hence, bias error will not be addressed in this study, except where obvious biases can be identified. However, it should not be construed that bias in the luminosity optical temperature measurements is insignificant. Rather, it will be kept in mind that bias errors may be significant. Thus, although in the present study "uncertainty" will be used to refer to the precision index, if biases can be a posteriori estimated through future work based on special calibrations, equation 3 can be directly reapplied with the system bias values to provide a true uncertainty.

Because gas temperature is not directly measured with the luminosity optical temperature system, but is determined as a function of calibration and measurement parameters, uncertainty in the gas temperature is really an effect of the propagation of the calibration and measured parameter uncertainties through the measurement function or relation. A truncated Taylor series method will be used to evaluate the uncertainty propagation.

2.0 THEORY OF TEMPERATURE UNCERTAINTY

2.1 Theory of Optical Emission Temperature Measurements

The optical emission temperature measurement system, also called the relative temperature measurement system and the luminosity system, determines the temperature of a combustion gas by measuring the thermal emission of the gas and using Planck's radiation law. Hereafter the measurement system will be referred to as the probe and the combustion gas will be referred to as the plasma.

The rate at which energy is radiated per unit area of surface at a given wavelength from a perfect thermal radiator (black body), is a function of wavelength and temperature and is given by Planck's law as [5]

$$e_{b\lambda}(T) = \frac{C_1}{\lambda^5[\exp(\frac{C_2}{\lambda T}) - 1]} \quad , \tag{4}$$

where $e_{b\lambda}$ is the wavelength specific black body emmision level (called the spectral radiance), C_1 is defined as 3.7418×10^{-5} erg cm^2/sec, C_2 is defined as 1.4388 cm K, λ is the wavelength of the emission measurement and T is the temperature of the black body. An MHD plasma, however, is not a perfect thermal radiator and therefore its emission is given by

$$e_{p\lambda} = \varepsilon_{p\lambda} \, e_{b\lambda} \quad , \tag{5}$$

where $\varepsilon_{p\lambda}$ is the wavelength specific emissivity or emittance of the plasma, $e_{p\lambda}$ is the spectral radiance of the plasma, and $e_{b\lambda}$ is the spectral radiance of a black body.

The probe uses a photodiode and an operational amplifier to monitor the incident radiant flux and convert it to a proportional voltage level. The probe also uses a narrow wavelength bandpass filter to limit the measurements to a specific spectral bandwidth of the radiant flux density. The wavelength specific spectral radiance of the plasma can then be related to the output in volts of the probe by the equation

$$e_{p\lambda} \cdot \tau = (K_1 \cdot V + K_0) \quad , \tag{6}$$

where $e_{p\lambda}$ is the plasma spectral radiance, τ is a radiation transmission factor, K_1 and K_0 are calibration constants, and V is the probe output voltage. To simplify calibrations, constants τ, K_1 and K_0 are combined resulting in the equation

$$e_{p\lambda} = (A1 \cdot V + A1). \tag{7}$$

Using the results of equations 5 and 7 in equation 4 gives

$$[A1 \cdot V + A1] = \frac{C_1 \; \varepsilon_{p\lambda}}{\lambda^5 [\exp(\frac{C_2}{\lambda T}) \; -1]} \quad . \tag{8}$$

Solving for the temperature in equation 8 yields

$$T = \frac{C_2}{\lambda} [\ln [\frac{C_1 \; \varepsilon_{p\lambda}}{\lambda^5 (A1 \cdot V + A0)} + 1]]^{-1} \quad . \tag{9}$$

So the temperature of the plasma is a function of the variables λ, $\varepsilon_{p\lambda}$, A1, A0, and V.

All the parameters in equation 9 are physical constants, calibration constants, or measured parameters for each specific probe system with the exception of $\varepsilon_{p\lambda}$, the spectral emissivity of the plasma. Thus the probe system makes one measurement, of V (voltage), that depends on two unknowns, T and $\varepsilon_{p\lambda}$. As a result the probe system cannot alone provide a unique determinant (or "absolute") measurement of plasma temperature. However, if the plasma spectral emissivity can then be estimated or defined separately, then the probe system can provide "relative" plasma temperatures.

The spectral emissivity of the plasma is influenced by many different parameters of the flow. These include detected wavelength, concentration of species emitting at that wavelength, broadband emitting slag particulate concentration and distribution, and other factors about which little information is known or can be derived by simple methods. However, it is possible to select a probe measurement wavelength band in which strong plasma species emission should predominate over other emissions, and with other measurements for similar gas conditions it should be possible to place somewhat restrictive bounds on the plasma spectral emissivity. By using a strong species emission line, even if other measurements cannot be made to bound the spectral emissivity, an assumption that the plasma emissivity has a significant value and is constant over a small spatial region of the plasma or is constant over a short time period, provides the bounds necessary to measure spatial or temporal temperature variations with the probes. Fortunately, the primary purpose of the optical probes is to obtain relative temperature measurements, and/or to determine the relative temperature fluctuation levels in magnitude and frequency. Hence, if the emissivity can be assumed to be sufficiently large that gas emissions, not wall emissions, are being measured, and if the emissivity can be assumed to be spatially constant over the small region of measurement, then plasma temperature profiles can be deduced that are not effected by error in the assumed value of the emissivities.

2.2 Theory of Uncertainty Values

To determine the uncertainty in the calculated relative temperatures it is necessary to analyze the uncertainties of the various independent variables. The uncertainty in T, ΔT, can be given as a function of the uncertainties of the independent variables (e.g. ε_λ, V, λ) by evaluating changes in the temperature measurement that result from perturbations in the independent variables.

The selected standard uncertainty analysis technique uses a truncated Taylor series expansion to evaluate changes in a measured parameter due to a perturbation in a variable (x) in the function used to determine the measured parameter [6]. The changes in the measured parameter f(x,y,z) due to a perturbation, δ, in the x variable is given by,

$$\Delta fx = F(x + \delta, y, z, \ldots) - F(x, y, z, \ldots)$$
$$= \delta \frac{\delta}{\delta x} (F(x,y,z, \ldots)) \quad . \tag{10}$$

For the probe system, equation 9 for temperature can be expanded in a similar truncated Taylor series for evaluation of the temperature uncertainty, ΔT, due to possible perturbations (uncertainties) for each of the variables. Then, assuming that the temperature uncertainty due to each variable uncertainty is not dependent or correlated with any other variable uncertainty, it is possible to obtain an overall maximum uncertainty. This maximum uncertainty is the summation of the uncertainties caused by each independent variable. Based on the temperature relation of the probe, equation 9, and the uncertainty procedure of equation 10, the maximum uncertainty in T is given by

$$\Delta T_{max} = |\Delta T_{\lambda}| + |\Delta T_{\varepsilon}| + |\Delta T_{A0}| + |\Delta T_{A1}| + |\Delta T_{V}| \quad . \tag{11}$$

It is assumed that this maximum uncertainty will overestimate the true measurement uncertainty, since intuitively, it seems highly probable that the uncertainties in each variable will produce non-additive changes in the measured temperature. Therefore it is useful to define a probable measurement uncertainty for the probe temperature based on equations 9 and 10. This probable temperature measurement uncertainty is given by

$$(\Delta T_{prob})^2 = (\Delta T_{\varepsilon})^2 + (\Delta T_{\lambda})^2 + (\Delta T_{A0})^2 + (\Delta T_{A1})^2 + (\Delta T_{V})^2 \quad . \tag{12}$$

The terms of equations 11 and 12 are be defined using equation 10 and differentiating equation 9, to obtain, for example,

$$\Delta T_\varepsilon = \delta_\varepsilon \frac{\partial}{\partial \varepsilon} \{\frac{C_2}{\lambda} [\ln(\frac{C_1\ \varepsilon}{\lambda^5(A1 \cdot V + A0)}) + 1)]^{-1}\} \quad (13a)$$

$$= \delta_\varepsilon \{ \frac{\frac{-C_2\ C_1}{\lambda^6(A1 \cdot V + A0)}}{[\ln(\frac{C_1\varepsilon}{\lambda^5(A1 \cdot V + A0)} + 1)]^2 \quad [\frac{C_1\varepsilon}{\lambda^5(A1 \cdot V + A0)} + 1]} \} \quad .$$

Thus, similarly,

$$\Delta T_\lambda = \delta_\lambda \{ \frac{-C_2}{\lambda} [\ln(\frac{C_1\varepsilon}{\lambda^5(A1 \cdot V + A0)} + 1)]^{-1}\} \quad \cdot$$

$$\{ \frac{\frac{-C_1\varepsilon\ (5)}{\lambda^6(A1 \cdot V + A0)}}{\{[\ln\ (\frac{C_1\varepsilon}{\lambda^5(A1 \cdot V + A0)} + 1)]^2 \cdot [\frac{C_1\varepsilon}{\lambda^5(A1 \cdot V + A0)} + 1]\}} \} \quad (13b)$$

,

$$\Delta T_{A0} = \delta_{A0} \{ \frac{-C_1[\ln(\frac{C_2\varepsilon}{\lambda^5(A1 \cdot V + A0)} + 1]^{-2} \cdot [\frac{C_2\varepsilon}{\lambda^5}]}{\lambda[\frac{C_2\varepsilon}{\lambda^5(A1 \cdot V + A0)} + 1] \cdot [A1V + A0]^2} \} \quad (13c)$$

,

$$\Delta T_{A1} = \delta_{A1} \{ \frac{-C_1[\ln(\frac{C_2\varepsilon}{\lambda^5(A1 \cdot V + A0)} + 1)]^{-2}\ [\frac{C_2\varepsilon}{\lambda^5}]}{\lambda^5[\frac{C_2\varepsilon}{\lambda^5(A1 \cdot V + A0)} + 1]\ [A1 \cdot V + A0]^2} \quad (13d)$$

,

and

$$\Delta T_V = \delta_V \{ \frac{-C_1[\ln(\frac{C_2\varepsilon}{\lambda^5(A1 \cdot V + A0)} + 1)]^{-2} \cdot [\frac{-C_2\varepsilon\ A1}{\lambda^5}]}{\lambda^5[\ \frac{C_2\varepsilon}{\lambda^5(A1 \cdot V + A0)} + 1]\ [A1 \cdot V + A0]^2} \} \quad (13e)$$

.

Equation 11 or 12 were used with equation 13 to determine what effect uncertainties in the independent variables have upon the maximum uncertainty and most probable uncertainty of T, the measured variable, based only on measurement system precision indices. The task of determining overall uncertainty in T requires that bias uncertainties be determined also, and then used with the precision indices to evaluate equation 3. However, in this report the task of determining uncertainty in gas temperature is reduced to a task of defining precision uncertainties for the independent variables and their effect on temperature uncertainty. In the actual probe application, it is necessary to take great care during probe use to reduce or eliminate sources of bias.

2.3 Reference Values Used in the Analysis

For the purpose of evaluating the uncertainty in the measured temperature, T, it is necessary to assume some values for the independent variables upon which T depends. The values for the emissivity, voltage, and calibration constants were derived from tests conducted in th CFFF. The LMF1E test series which was conducted in the Fall of 1983 was used to obtain the values. A value of .80 was decided on as a "best guess" for the emissivity based on (a) emissivity measurements done at a point in the flow train downstream of the nozzle and MHD channel called the diffuser exit (see figure 1), and (b) previous measurements made in the combuster of a similar UTSI MHD flow train [3]. A value of 1 volt was found to be a good average for the probe output voltage during these tests. The calibration constants A0 and

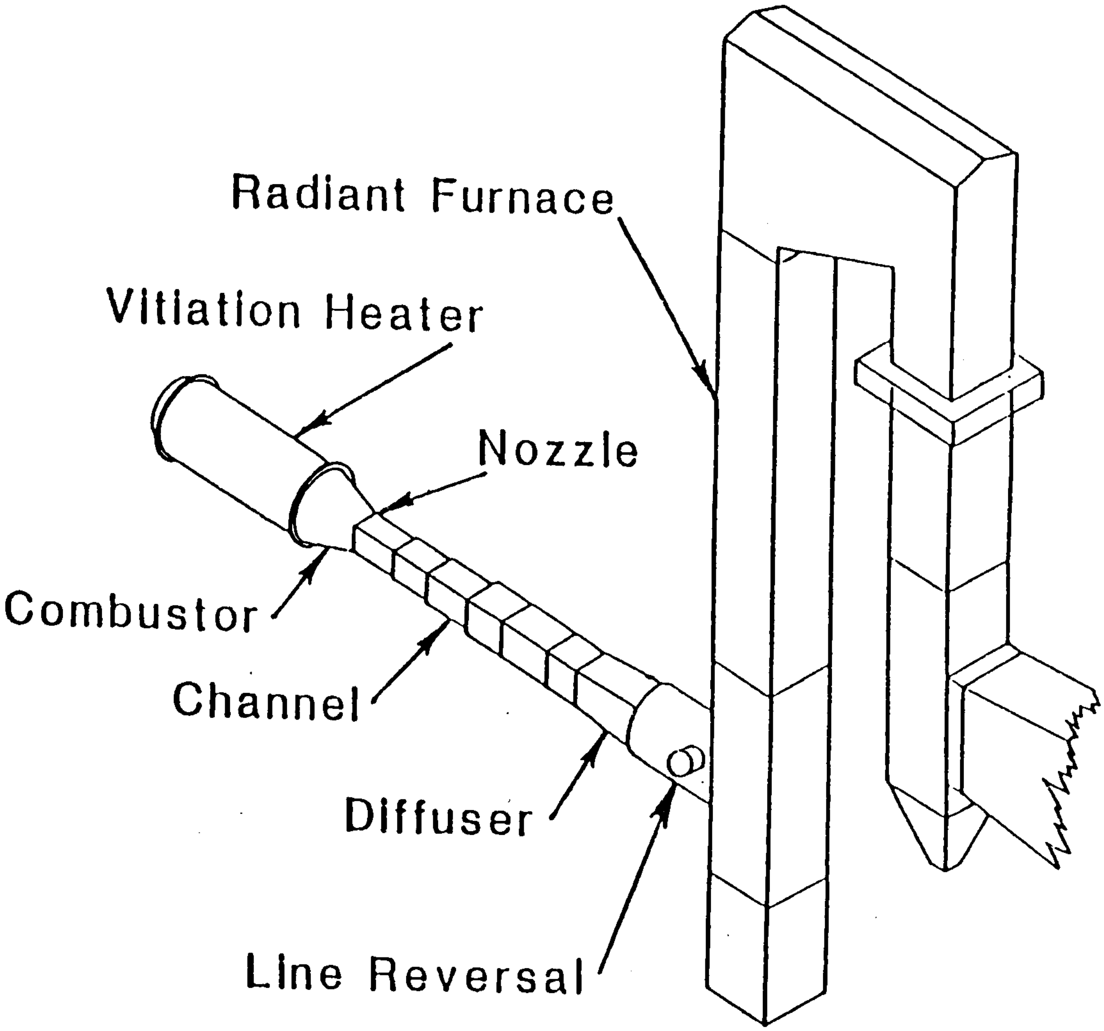

Figure 1. CFFF Flowtrain.

$A1$ were determined from the voltage values from a probe on the flowtrain centerline during test LMF1E1, and are given by 0.4486 x 10^{-13} cm^3·sec/erg and 0.1662 x 10^{-13} cm^3·sec/erg·volt respectively.

The remainder of the independent variables in equation 11 were not dependent on the test series. The measurement wavelength chosen was 750 nm, the center of the 1 nm bandpass interference filters used in the luminosity optical system, and the constants C_1 and C_2 are, respectively, 3.7418 x 10-5 erg·cm/sec and 1.4388 cm·K.

Using the above values and equation 13, equations 11 and 12 can be rewritten as

$$\Delta T_{max} = 447.22 \,|\,\delta e\,|\, + 90.79 \,|\,\delta V\,|\, + 545 \times 10^{-13} \,|\,\delta A1 + \delta A0\,|\, + 5.617 \times 10^{7} \,|\,\delta\lambda\,|\,, \qquad (14)$$

and,

$$(\Delta T_{prob})^2 = 2 \times 10^5 (\delta\varepsilon)^2 + 8.24 \times 10^3 (\delta V)^2 + 2.98 \times 10^{31}[(\delta A1)^2 + (\delta A0)^2] + 3.156 \times 10^{15} (\delta\lambda)^2. \qquad (15)$$

As mentioned before, C_1, and C_2 are constants and do not contribute to the temperature uncertainty except through the coefficients of equation 15. In actuality these constants do have "uncertainties", however these uncertainties are very small. C_1 has a value of 3.7418 x 10^{-5} erg·cm^2/sec and an uncertainty of 1.75 x 10^{-12} erg·cm^2/sec. C_2 has a value of 1.4388 cm·K and an uncertainty of 3.34 x 10^{-5} cm·K. These uncertainties in C_1 and C_2 would result in a 0.002% uncertainty in temperature using the values given above for the other parameters.

This uncertainty is insignificant in relation to the uncertainty introduced by the other parameters and therefore these constants can be assumed to be truly constant.

δT_{max} as stated in equation 14 is actually the precision index in T, the precision index being defined previously. This means , since we are assuming the bias to be zero, that all of the independent parameters must be precision indices. The precision index of the emissivity and voltage is simply the standard deviation of these parameters since their standard deviations were calculated from more than thirty data points. In fact these parameters' standard deviations were calculated from hundreds of data points. The precision index in the wavelength is defined by the manufacturer and their definition of its precision index is considered to be correct. The precision index for A1 and A0 is not adequately defined by the standard deviation in these paramenters because only four data points were available due to equipment difficulties. The source used for this work was a primary standard NBS traceable source. To use the standard deviations obtained from four data points, it was necessary to assume the 95% point from the Student's t distribution for three degrees of freedom, 3.182, instead of the factor of two in equation 2. This was done so that the standard deviations in the calibration constants could be used consistently along with the other parameters' standard deviations. It can be shown that the standard deviations in the calibration constants must be multiplied by a factor of 2.53 to be used in equation 15 to maintain a uniform definition for all the parameters for the 95% confidence level in the temperature uncertainty.

These factors, constants, and uncertainties are discussed in greater detail in Section 4.2 where their numerical values are justified on the basis of overall system operation.

3.0 ANALYSIS OF SPATIAL RESOLUTION UNCERTAINTIES

3.1 Factors That Affect Spatial Resolution

When analyzing the luminosity optical probe system for relative gas temperature uncertainties it is necessary to consider not only the precision index uncertainties of the measurement system, but also the influence of uncertainties in the spatial resolution. Spatial relative temperature profiles can obviously be affected by the uncertainties in the spatial location of the measurement. Also, the uncertainty in the spatial extent of the measurement will introduce uncertainty in the measurable frequency band for temporal relative temperature variations. The maximum measurable frequency is defined by the velocity of the plasma divided by the spatial extent of the measurement. Therefore uncertainty in the probe's spatial resolution creates an upper frequency boundary. This upper frequency bound will be discussed in more detail in section 4.2.

The spatial resolution uncertainty, however, is distinct from the previously derived precision index uncertainties because uncertainties in the spatial resolution are either fixed, as in the resolving capabilities of the probe, or are biases which need to be eliminated by careful design of the probe system and careful installation and operation of the probes. This resolving capability is a precision index but is not defined by a standard deviation but is rather a fixed quantity. For example, if the probes look at collimated light emissions from a 3 mm diameter cylinder of plasma, then the spatial location of the measurement can be defined to be at the center of this cylinder with a totally definable spatial uncertainty (precision index) or resolution of ±1.5 mm. However, if two probes are installed 20 mm apart, but one probe is tilted 10 degrees to the centerline of the other probe, the spatial resolution uncertainty in the measured relative temperature profile will have a spatial uncertainty bias component equal to the optical depth of the measurement multiplied by sin(10°). Possible biases such as these need to be identified so that they can be eliminated, as this example bias can be eliminated simply by proper probe installation.

In the CFFF application there are basically three factors which can produce spatial uncertainty bias. The first, and simplest to eliminate, is improper installation of the probes, such as the tilted installation mentioned above, or improper assembly resulting in an internal bend in the probe. This factor will be assumed to be eliminated by proper assembly and installation and will not be discussed further. The second factor to be considered as a potential cause for spatial bias is the effect on the measurement spatial resolution of the line of sight path measurement that is being made. When making relative temperature profile measurements it is important to make the measurements in the same plane, perpendicular to the probe axes, and line of sight measurements may not satisfy this criteria. The third factor is the probe specific capability of the probe optical structure to collimate the light being detected, with consideration of decollimating effects due to internal probe reflections.

3.2 Effects of Line-of-Sight Averaging

Ideally, line of sight plasma temperature measurements would be made so that the probe axes were viewing parallel to plasma conditions which were homogeneous. Then the relative contributions to the probes' signals would be the same from each plane perpendicular to the probe axes which the probes "looked" through. In other words, ideally the plasma conditions should be constant across the flow. Since hot flows ducted through cooled walls (as exists in the CFFF flow) do not have an axis transverse to the flow along which the plasma conditions are homogeneous, the luminosity optical measurement will provide a non-linear "average" of the different plasma emission characteristics seen by each probe as the basis for temperature profile measurements. The resulting measurements can still be made representative of plasma conditions along a plane perpendicular to the probe axes and including the core, or more simply, representative of the core region.

Analysis of a similar MHD plasma temperature measurement which is known as the the emission-absorption (or line reversal) technique, provided criteria for selecting the measurement wavelength so the temperature measurement would be representative of the central hot core conditions [7]. These same criteria were directly utilized, due to the similarity of the measurement systems, in selection of the luminosity optical probe detection wavelength, as defined by the incorporated interference filter. Basically this criteria requires examination of the broadened and self reversed species line emissions for the gas species selected for the measurement.

3.3 Wavelength Selection

The potassium emission lines at 766.5/769.9 nm were the desired measurement region since this potassium doublet is very bright due to the significant addition of the seed, potassium carbonate, to the coal. A typical emission spectra for the CFFF plasma is shown in figure 2. The brighest portion of the doublet for the core flow, the 766.5 and 769.9 nm line centers, cannot be used for core representative temperature measurements because of self reversal (absorption) caused by the cool boundary layer regions near the walls. A measurement wavelength of 750 nm was chosen as the center of the 1 nm probe bandpass filter in part because it is near enough to the 766.5 nm line center that it has sufficient brightness to differentiate the gas phase potassium species emissions from the background radiation of the particulates and the far wall. The 750 nm wavelength was also selected because it is far enough away from the line center so that the absorption in the cool boundary regions has little effect on emissions at that wavelength. By choosing the 750 nm wavelength the boundary layer should not have an appreciable effect on the temperature measurement.

3.4 Effect of Probe Collimation on Measurement Accuracy

The third factor considered as a potential cause for spatial bias was the collimation characteristics of the probe design. Effects of this factor can be illustrated by considering an ideal probe. It would consist of two planes of infinite extent separated by an infinite distance so that there is no internal reflection and the photodiode in the probe 'sees' a perfect cylinder (see figure 3). Of course, this is not the case in actuality, and an example of a 'real' probe is shown in figure 4. This figure illustrates internal

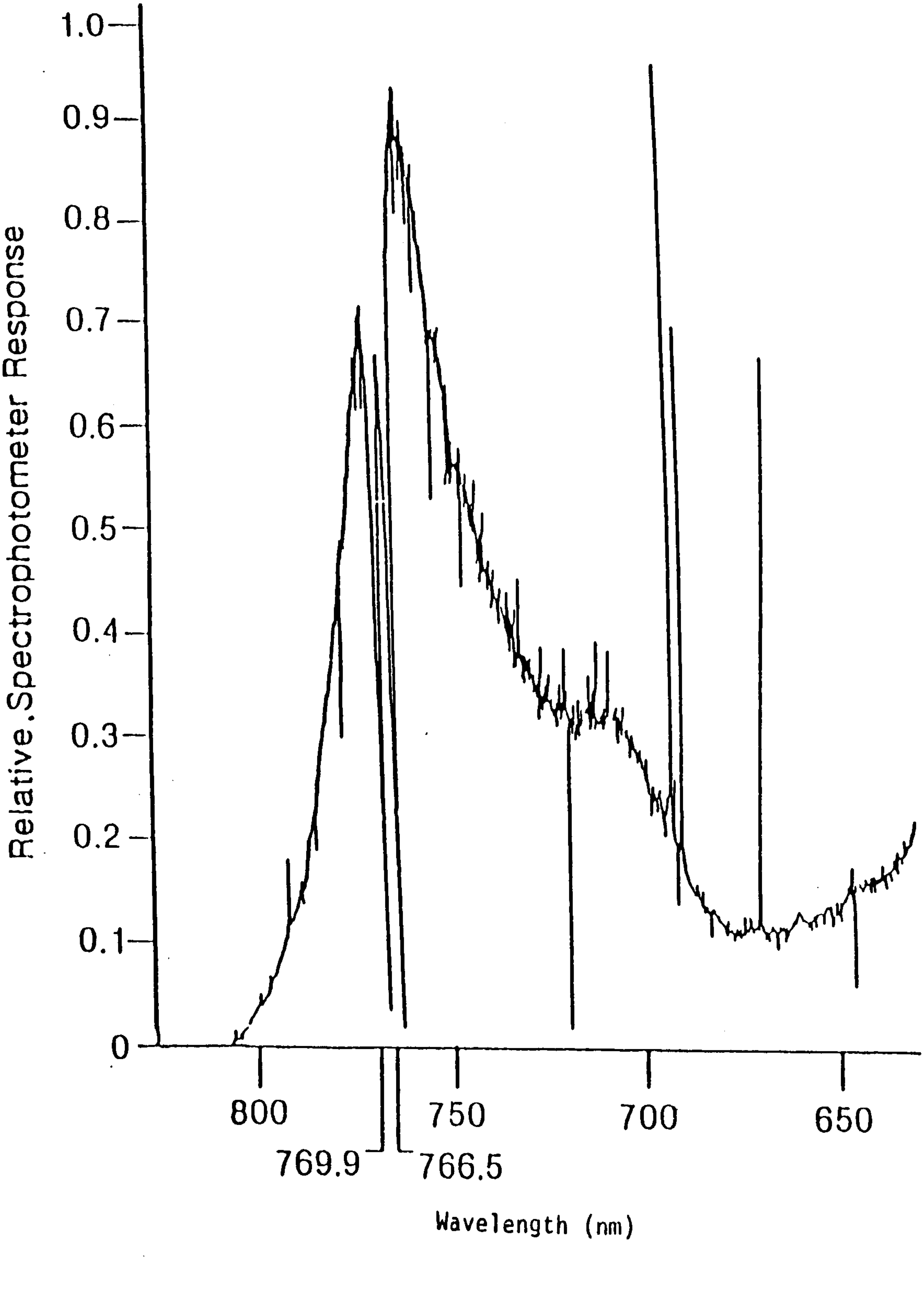

Figure 2. Spectral Emission of Coal+Potassium Plasma.

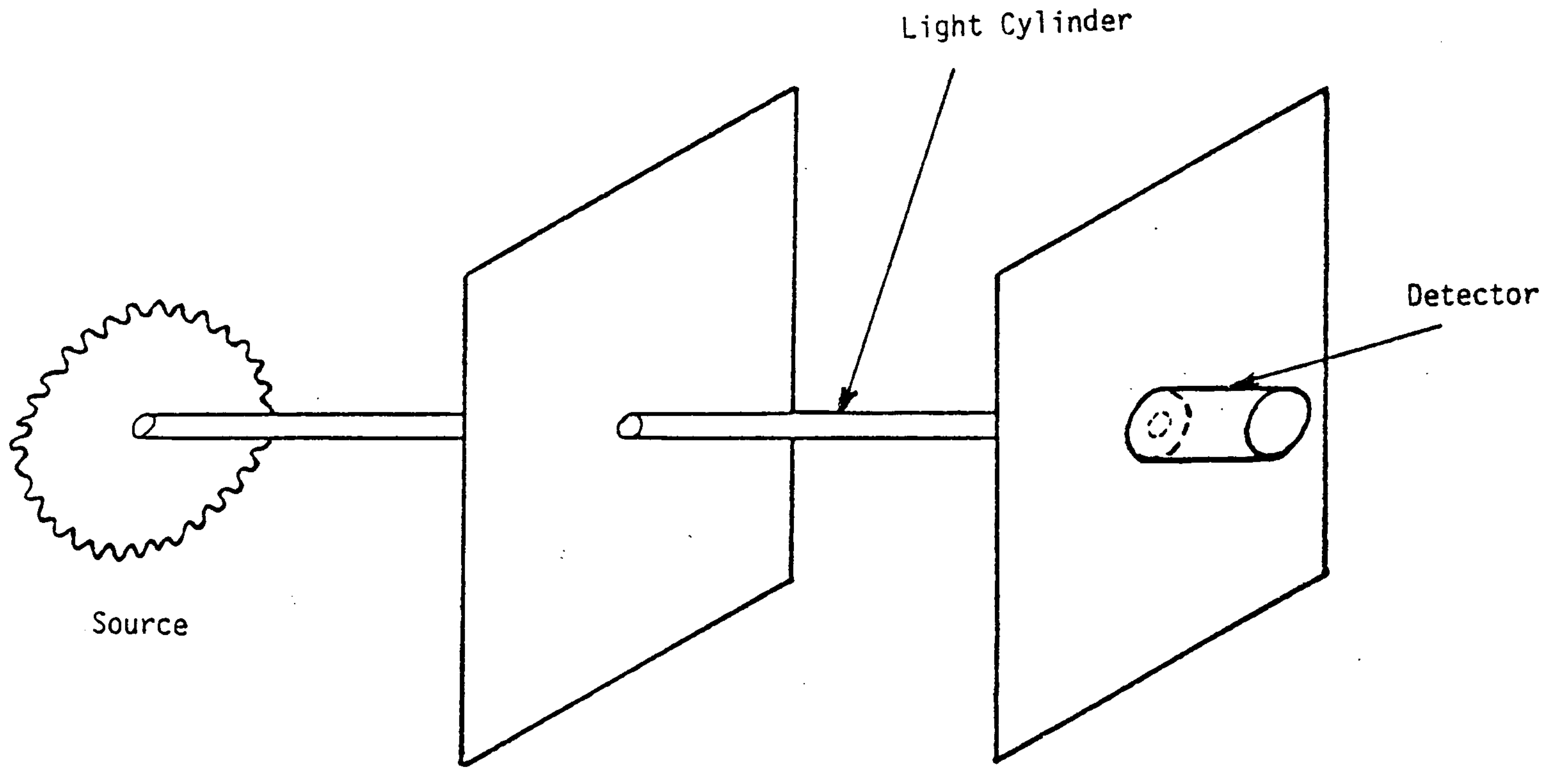

Two planes of infinite extent infinitely far apart illustrate a perfect probe design with no internal relfection and a perfect cylinder of light incident on the detector.

Figure 3. Theoretically Ideal Probe.

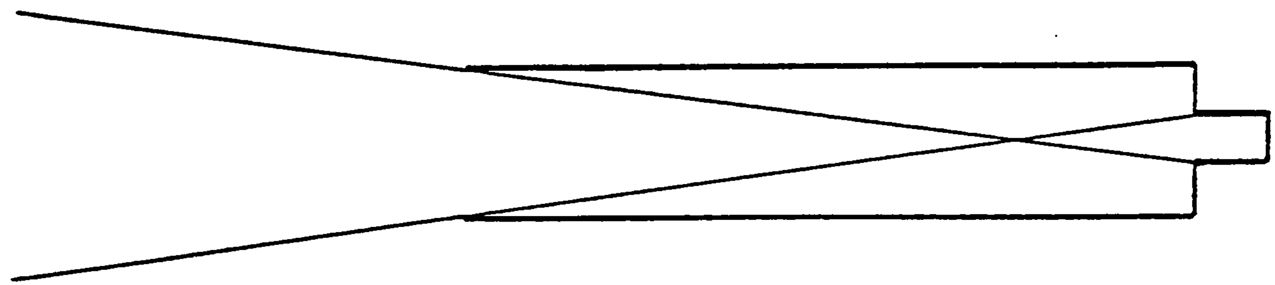

a) Divergent light cone viewed by the detector.

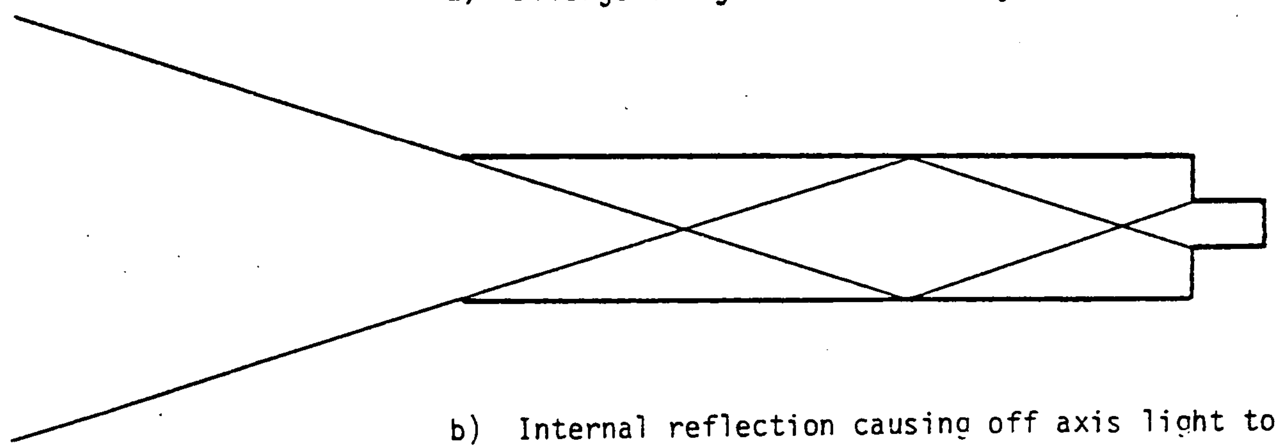

b) Internal reflection causing off axis light to reach the detector.

Figure 4. Problems of Real Probe Designs.

reflection and the cone of light incident on the photodiode. Or basically, the lack of collimation of the probe.

The lack of collimation, if it were large, could cause the probes to see overlapping regions of the plasma and would seriously effect the temperature profiles. Fortunately, the small physical size of the nozzle section, about 8 cm, leads to a small divergence angle for the light cone seen by the probe, thus, the divergence of the light cone entering the probe has little effect. The .33 cm diameter photodiode would see a circle with a diameter of about 1.5 cm if it could see across the nozzle section. The probes are separated sufficiently so that this amount of divergence results in a relatively small spatial resolution uncertainty compared to the space between probes.

3.5 Effects of Probe Internal Reflection on Measurement Accuracy

Unfortunately, internal reflection in the probe body is a much more difficult problem. In fact, a method has not been defined to determine to what degree internal reflection effects the temperature measurement's spatial resolution. It is obvious, however, that internal reflection would create a spatial resolution broadening causing the probes to receive radiation from regions outside of the entering light cone defined by the probe structure. Because of the difficulty in defining the effects of internal reflection and their possible large magnitudes an attempt was made to minimize internal reflection.

The first probe was constructed with the idea of using a straight bore down the probe body to collimate the light (see figure 5). After this probe was constructed it was found that it had severe internal reflection. Attempts to reduce the internal reflection were made by

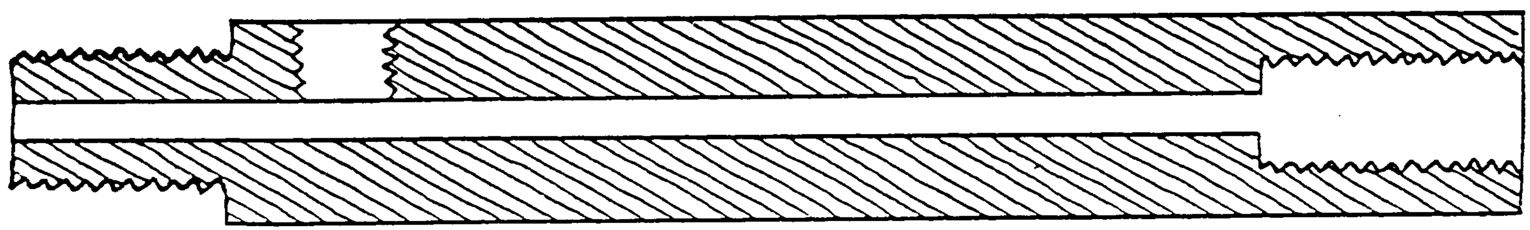

Figure 5. First Probe Design.

threading the internal bore, sandblasting the bore as much as possible, and applying a non-reflective paint to the inside of the probe. Because only a shallow thread could be cut in the bore, threading had little effect on reducing the internal reflections. Attempts at sandblasting the long, narrow bore were also not effective in significantly reducing the internal reflection. The paint did produce a significant reduction in the internal reflections but the paint would not continue to adhere satisfactorily to the stainless steel probe. The internal reflection problem became more severe when the probe had to be shortened to accommodate the geometrical constraints of the CFFF flowstream. Because of this internal reflection problem a new probe was designed.

3.6 Design of Optical Emission Probe to Minimize Internal Reflection

The new probe, also made of stainless steel, was designed to aid in reducing internal reflection (see figure 6). The new design incorporated a significantly larger bore which would allow deep threading of the probe's interior along most of its length. It was thought that this would act as multiple optical stops to reduce propagation of internal reflections. The new design also incorporated several small diameter optical stops placed within the larger probe bore to provide small light beam divergence while minimizing the reflective surface area adjacent to the collimated light path. This design, from simple examination, seemed much improved over the original but it was prohibitively expensive to construct. It was found to be very difficult to thread deep into the interior of the probe mainly due to the small

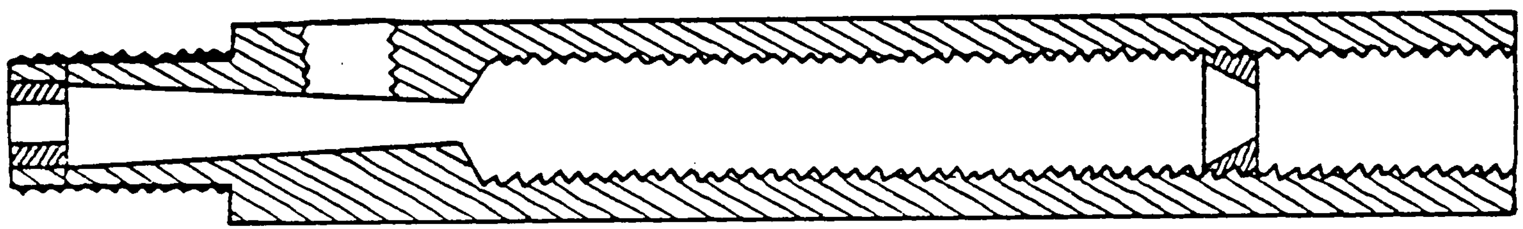

Figure 6. New Probe Design.

diameter of the probe, approximately one centimeter, and to the material of the probe, stainless steel, which is very difficult to machine. For these reasons this probe design was further modified.

The modified new probe design was to accomplish two things; one, to reduce internal reflection, and two, to be economically feasible to construct. It incorporated the optical stops as configured in the new design and it was shallow threaded approximately one third of its length to receive one of these stops. Instead of deep threading the entire length, however, it was sandblasted over the remaining two thirds of its length to create a rough surface to reduce internal reflection (see figure 7). This design is significantly easier and thus more economical to build. A probe installed in the CFFF nozzle throat is illustrated in figure 8 showing the placement of the filter and the photodiode. The task that remained was to define how significant the new designs were in reducing internal reflections when compared with the original probe, and each other.

In order to study this problem a source was constructed that would be evenly illuminated across its surface (see figure 9). The probes could then be placed in front of the source and moved away while the probe output was being monitored. In this way the internal reflection of each probe design could be studied. The internal reflection study is based on the fact that since a non-collimated source emits light in a conical segment of a sphere, as the probe is moved away from the source the radiant flux density incident on the photodiode decreases proportionally to the separation distance squared. Simultaneously, the area extent of the source seen by the detector

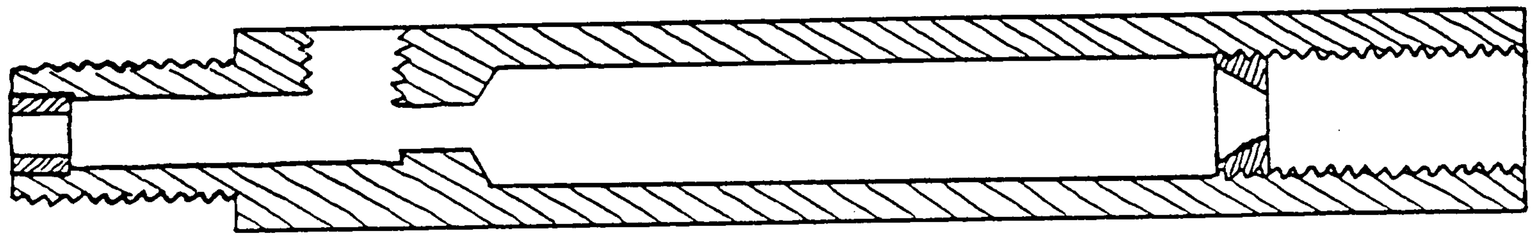

Figure 7. Modified New Probe Design.

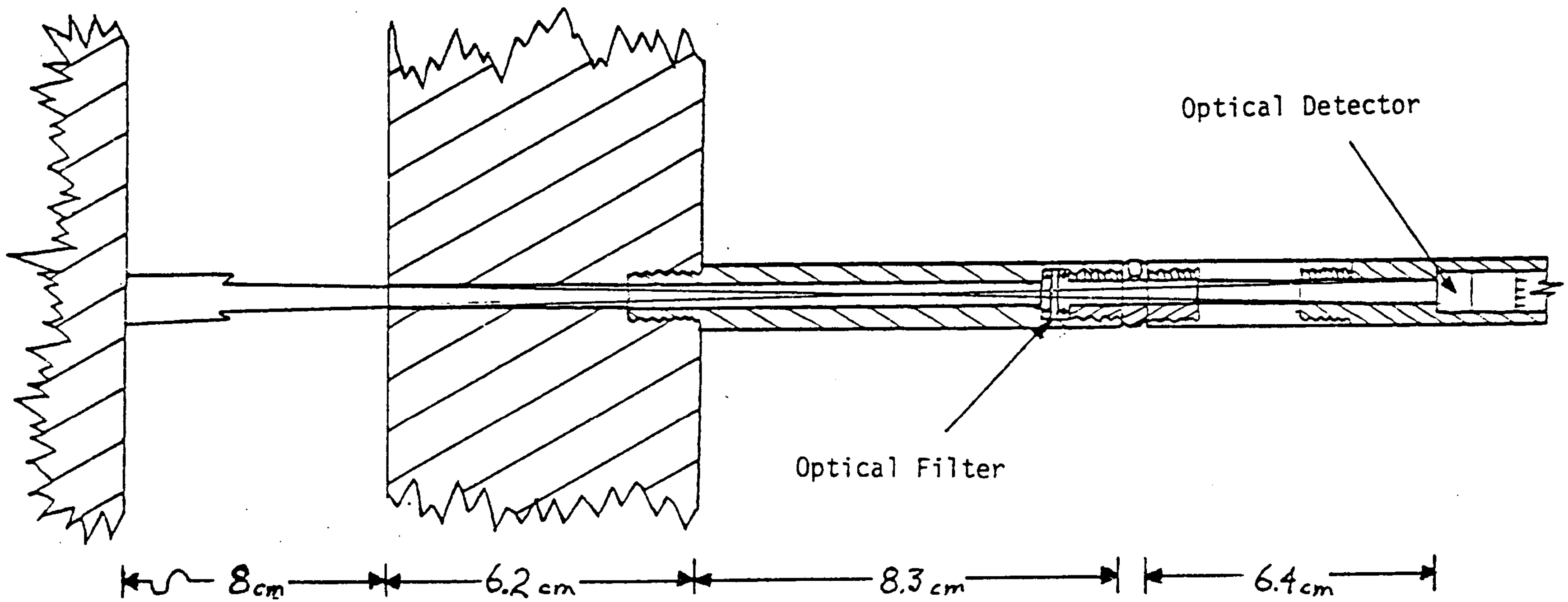

Figure 8. Installed Probe.

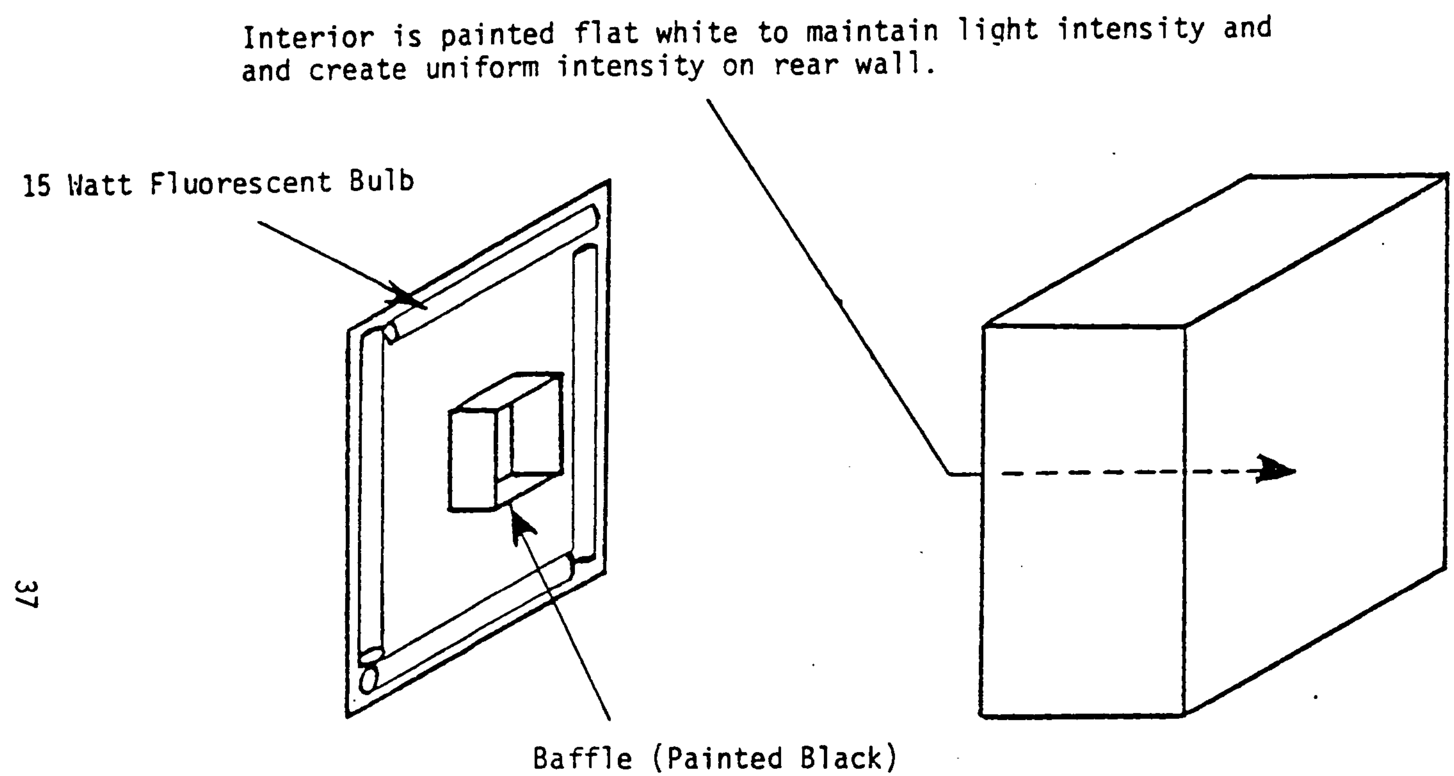

Figure 9. Experimental Source.

increases with the base of the cone of "collimated" light seen by the detector, which increases proportional to the separation distance squared. These two factors exactly cancel each other when the probe is truly collimating the light, so that, if the source is evenly illuminated and there is no internal probe reflection, the amount of radiation reaching the photodiode will remain constant as the probe is moved away from the source as long as the field of view of the probe is totally within the uniformly illuminated region of the source.

In testing the different probe designs for internal reflection the output voltage of each probe was measured at fixed distances away from the source. The degree of internal reflection was then determined by the amount these voltages differed. Figure 10 shows graphically how the internal reflection in the various designs effects the output. This data was obtained using the experiment described above.

As can be seen by figure 10 the modified (sandblasted) new probe design is much better than the original designs and slightly better than the new (threaded) design. In fact figure 10 shows that there is no measurable voltage change, and therefore no measurable internal reflection, at all in the modified probe design. Undoubtedly, there is some internal reflection in the modified design that was not measurable in the testing. The test source used four fifteen watt fluorescent bulbs and therefore did not emit much radiation. If the source had been very bright it is likely that some internal reflection effect would have been measurable, but this posible effect should not introduce significant uncertainty in the location of the probe measurements. Given the space limitations on the physical size of the

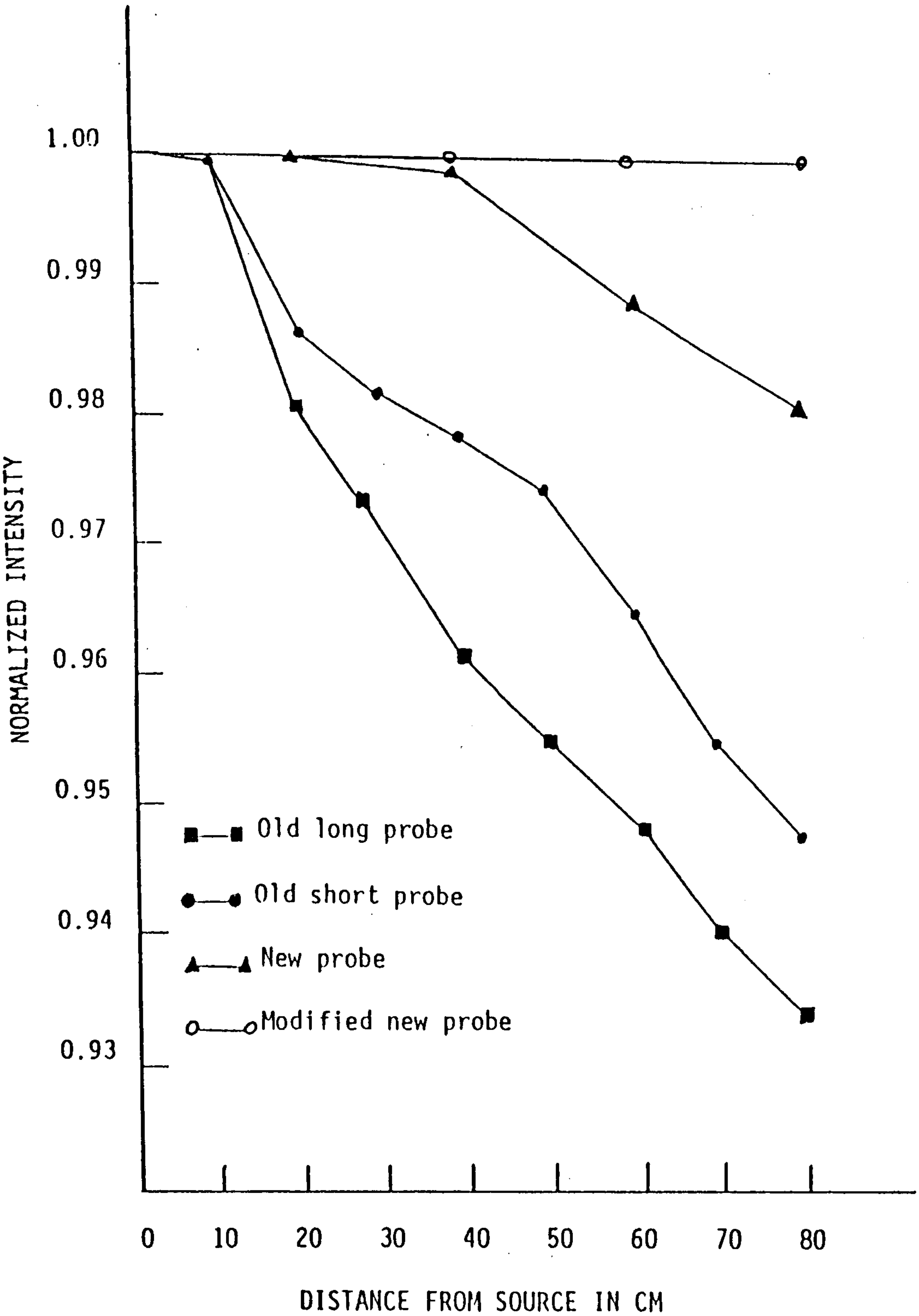

Figure 10. Relative Internal Reflection.

probe, however, the third probe design seems to do an excellent job of limiting internal reflection, and the amount of radiation that might reach the photodiode through the modified new probe from internal reflections, should not be enough to have a significant effect on the temperature profiles.

4.0 ANALYSIS OF UNCERTAINTIES CAUSED BY OPTICAL EMISSION MEASUREMENT SYSTEM

4.1 General Discussion

In this section the theoretical formulations of Chapter 2.0 will be used to evaluate the luminosity probe optical measurement precision index uncertainty levels. First, the uncertainty in the emissivity will be determined, next the uncertainties in V, A1, and A0 will be evaluated, and finally, the uncertainty in the wavelength will be found. Then the overall precision index uncertainty propagation to the temperature measurement will be evaluated, using equations 14 and 15, and, finally, the spatial resolution of the probe system will be reviewed. As discussed in Chapter III spatial resolution problems can generate biases which in general need to be eliminated. It was shown that probe design and care in implementation should effectively eliminate the potential spatial resolution biases. In addition, the precision uncertainty of the probe spatial resolution was defined from the cone of light viewed by the probe in the absence of internal reflection.

For most of the parameters involved in temperature determination it is relatively straightforward to define what their uncertainty is. For example the voltage uncertainty, which will be discussed later, is simply determined by repeatedly measuring the voltage output while the probe is under constant illumination by a calibrated reference source. The standard deviation in the probe voltage is the voltage uncertainty.

Unfortunately, all the parameter uncertainties are not that easy or simple to define. The uncertainty in the emissivity is one such parameter.

4.2 Emissivity Precision Uncertainty

The emissivity uncertainty depends on variations in emissivity temporally and spatially. Spatial variations are important since the emissivity is assumed to be constant across the flow both along the line of sight view of the probe and between probes when spatial temperature variations are to be measured. Temporal variations are important since the emissivity is assumed to be constant during the measurement interval when temporal temperature variations are to be measured. In order to determine what value the emissivity uncertainty should have it is necessary to examine uncertainties for both types of variations.

Spatial variations in the emissivity at the nozzle throat would most likely be caused by spatial nonuniformity of the plasma constituents such as spatially varying potassium concentration. This could be caused by incomplete mixing in the combustor. Or, it could be caused by migrations of plasma constituents to different spatial regions in the nozzle. Particulates in the plasma are one "constituent" that will tend to migrate away from the nozzle walls and into the core flow region [8].

In addition to these difficulties in determining spatial variations there are similar difficulties encountered when defining temporal variations. Temporal variations in the plasma emissivity could be caused by irregularities in the coal or oxidizer flow rates to the combuster or the random nature of the turbulent mixing in the combustor, among other factors. These uncertainties could be determined simply if there were some way of measuring absolute emissivity at the nozzle. Unfortunately, with the existing hardware there is no way of actually measuring the emissivity at the probe location. Consequently there is no way to determine emissivity variation from test results. We are forced to assume emissivity uncertainties either from theoretical calculations or data obtained at other locations. The theoretical calculations necessary to obtain emissivity require knowledge of a number of plasma properties which also are not amenable to measurement so an attempt has been made to estimate emissivity uncertainty from data obtained at the diffuser exit. The diffuser exit is the closest location to the nozzle where emissivity has been measured in the CFFF flowtrain (see figure 1).

The mean and the standard deviations in the emissivity at the diffuser exit were determined from data taken during tests LMF1E2 and LMF1E3 in order to approximate the variations in the emissivity at the nozzle. At the diffuser exit a line reversal temperature measurement system was used to determine the emissivity from a line of sight view across the center of the flow. The two LMF1E tests were chosen because 1E2 had a very rough coal+potassium flow and 1E3 had a relatively smooth coal+potassium flow. It was thought that variations in potassium flow would have a strong influence on the standard deviation of the emissivity. This, however, was found to be untrue. The standard deviations of the emissivity were found to be 7.0 and 4.7 percent for the rough and smooth coal flow respectively. This indicates that the emissivity is not strongly dependent on coal/potassium flow variations and that the emissivity at the diffuser exit is reasonably constant with respect to time.

It is difficult to tell how the emissivity uniformity at the diffuser exit is related to the emissivity uniformity at the nozzle. It can be assumed that the emissivity at the diffuser exit is more uniform because other flow properties such as pressure and Mach number will exhibit considerably smaller gradients at the diffuser than at the nozzle. Differences between the nozzle and diffuser properties should not be extreme, however, and the low errors found at the diffuser exit suggest that the variations at the nozzle should be fairly low. Based on the fact that at the diffuser exit the emissivity ranges from .60 to .75 where the plasma is cooler, the emissivity at the nozzle will be assumed to be around .80. A worst case estimate for the emissivity variation uncertainty at the nozzle will be assumed to be plus or minus .1 or a relative error of about 12.5 percent. This is an 80% increase over the maximum emissivity uncertainty indicated from temporal variations at the diffuser exit.

The data obtained at the diffuser exit, while providing a measure of the temporal variations in emissivity, actually tells us very little about spatial variations at the diffuser exit. Furthermore, because of the different flow conditions at the nozzle (transonic, unidirectional) and the diffuser (subsonic, recirculating) spatial variations would not be expected to be similar at the two locations. In fact, there is no way to determine the spatial uncertainties in the emissivity at the nozzle throat with currently available equipment.

In view of the lack of data on which to base spatial emissivity uncertainties, for the purpose of uncertainty analysis we are assuming that the spatial emissivity uncertainty can be estimated as equal to the temporal emissivity uncertainty.

4.3 Precision Uncertainties in the Voltage and Calibration Constants

Fortunately, the uncertainties in V, A1, and A0 are more straight forward to determine than the emissivity uncertainty. These parameters are discussed together because the same method is used to evaluate these uncertainties. This method involves calibrating the probes many times. The calibration program determines what values A1 and A0 have for that particular probe being evaluated. The calibration is done by illuminating the probe with a reference source . The source radiance has been determined from optical calibrations performed with traceability to the National Bureau of Standards. The predicted response of the probe has also been calculated. This predicted response is entered into the calibration program along with the actual probe output while the probe is being illuminated by the source. Then, the probe tip is blocked so that no radiation can enter to establish the probe output for a zero radiance value. A0/A1 represents the zero intercept and A1 represents the linear slope of the probe response.

The uncertainty in these parameters is determined, as mentioned before, by carrying out the calibration procedure many times to establish the standard deviation in the various values of V, A1, and A0. In this manner the uncertainty in V was found to be 0.0021 volts with a mean of 2.6881 volts for an uncertainty of 0.079 percent. The uncertainty in A1 was found to be 0.0007 cm^3sec/erg-volt with a mean value of -0.2105 cm^3sec/erg-volt for an uncertainty of 0.33 percent. The uncertainty in A0 was found to be 0.00022 cm^3sec/erg with a mean value of 0.0978 cm^3sec/erg giving an uncertainty of 0.22 percent.

4.4 Precision Uncertainty of the Wavelength

The determination of the uncertainty in the wavelength, while differing from the procedure above, is similarly straightforward. The uncertainty in the wavelength is caused by two factors. One is the inherent bandpass of the optical filter used. The other is a possible wavelength bandpass shift caused by radiation incident on the filter at an angle other than ninety degrees. The filter used is an interference type and has a bandpass, full width at half maximum, of 1 nm with an uncertainty of .3 nm. This would yield a worst case uncertainty of 1.3 nm in the wavelength, due to the bandpass of the optical filter.

The wavelength uncertainty due to any wavelength shift depends on the filter transmission characteristics for varying incident radiation angles, as defined by the equation

$$\lambda_\theta = \lambda_0 [1 - \left[\frac{\text{Sine}(\theta)}{n_e}\right]^2]^{1/2} \qquad , \qquad (16)$$

where θ is the incident angle measured from the perpendicular, n_e is the effective index of refraction of the filter, λ_0 is the center wavelength of the filter, and λ_θ is the resultant wavelength [9].

Since, as was shown before, there is essentially no measurable internal reflection in the new probe, the angle θ in equation 16 is determined only by the narrow cone of light accepted by the probe body. This would cause a worst case incident angle of 1 degree. Since the filter that is used has an effective index of refraction, n_e, of 2.1, a θ of 1° would yield a wavelength uncertainty of 0.03 nm, which is negligable compared with the bandpass uncertainty of 1.3 nm.

4.5 Summary of System Precision Uncertainties

In summary, predicted uncertainties are 0.1 for the emissivity, 0.0021 volts for the voltage, 0.0007 cm^3sec/erg-volt for A1, 0.00022 cm^3sec/erg for A0, and 1.3 nm for the wavelength. Using these values for the various precision indices, with A1 and A0 multiplied by the factor 2.51 from equation 15, results in a probable precision index of 45.22 K for the temperature. This yields, from equation 3, a temperature uncertainty of ±91 degrees Kelvin since bias has been considered to be insignificant. This translates into a ±3.6% uncertainty in T.

4.6 Discussion of the Uncertainty in Relative Temperature Measurements

In presenting luminosity temperature measurements both this temperature measurement uncertainty of ±3.6% and the spatial uncertainty of the measurement need to be specified. As shown in Chapter 3.0 it should be possible to obtain a spatial resolution of half the probe aperture since internal reflection has been practically eliminated and the divergence of the light cone is very small. This would result in a spatial uncertainty of ±1.6 mm. This spatial resolution corresponds to a maximum resolvable frequency of temperature fluctuations of 1.6 MHz for the expected M = 1 nozzle velocity of 5200 m/sec. This is a very large frequency for sampling purposes. However, not all locations where the optical emission system might be used would have this small a cross section and high a velocity. For example, this system has been used in the past at the CFFF for diagnostics at the radiant furnace, a location downstream of the generator channel. At the radiant furnace meaurement points the duct was sufficiently wide and the flow sufficiently slow that a maximum resolvable frequency of 600 Hz results. Therefore, this factor could be of importance in some applications. Figure 11 illustrates the magnitude of the spatial uncertainties and the temperature uncertainty for various flow conditions for the LMF1 test series at the CFFF.

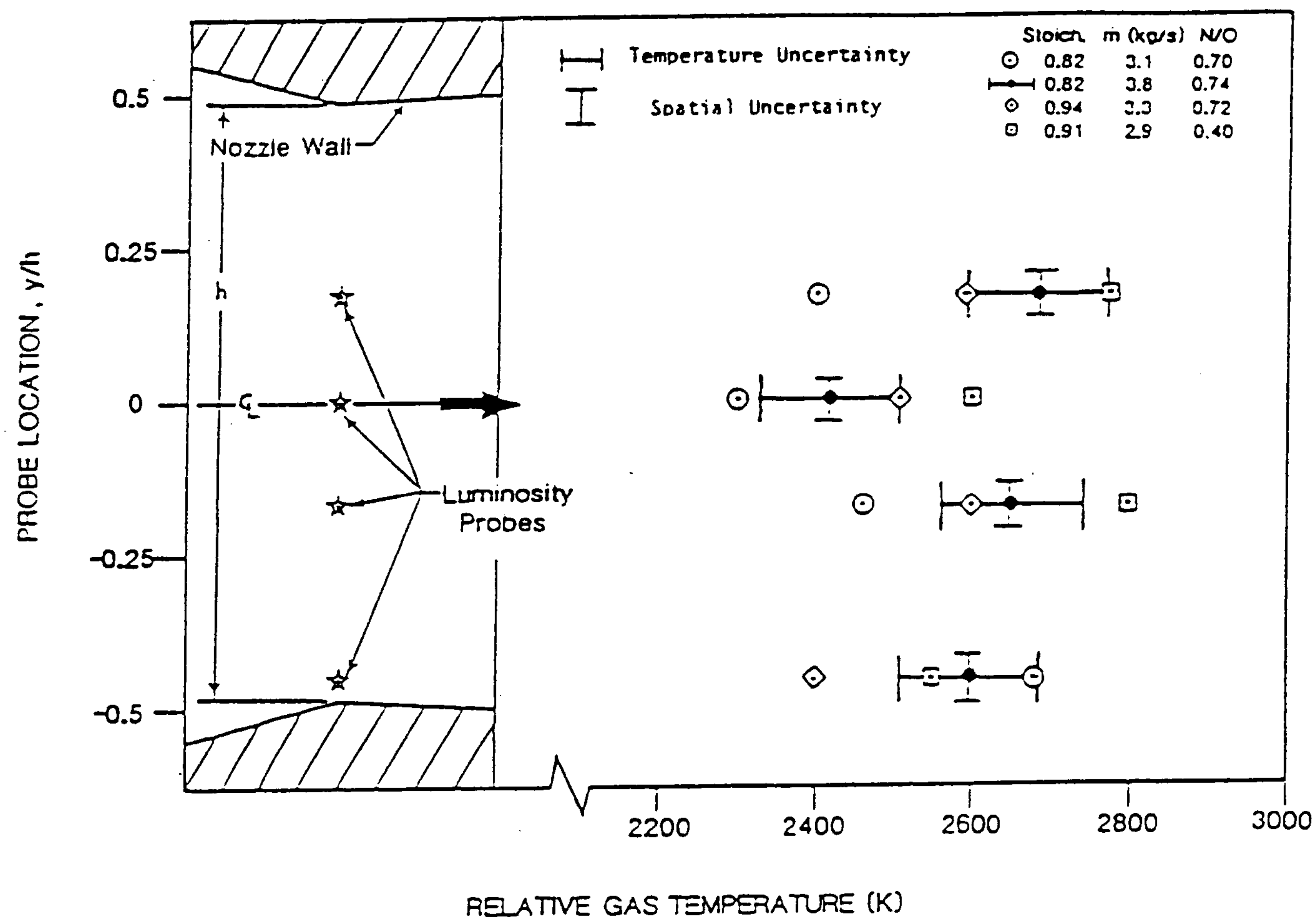

Figure 11. Spatial and Temperature Uncertainties..

5.0 SUMMARY AND RECOMMENDATIONS

5.1 Summary

Luminosity temperature probes have been used for some time to determine temperature profiles in coal fired MHD plasmas at the CFFF. Unfortunately, the uncertainties of the probe system were never accurately defined and therefore the temperature profiles obtained were questionable. This work was intended to define the uncertainties of this system. Basically, two areas were addressed: the measurement uncertainties and the spatial resolution uncertainties.

The uncertainties in the optical emission temperature measurement system were analyzed and the accuracy of the system for spatial temperature profiles at the nozzle throat of an MHD system was determined based on this analysis. The uncertainties in the spatial resolution were addressed and it was determined that these uncertainties can be minimized in terms of the probe optical view width by careful probe design and installation, which eliminates bias uncertainties. Internal reflection was shown to be a significant source of unknown bias in spatial resolution, and was addressed by redesigning the probe. The modified, new probe design was shown by testing to effectively eliminate internal reflection problems. These probes are currently in use at the CFFF, and provide a spatial resolution of ±1.6 mm. The uncertainties in the measurement system were determined and these uncertainties were shown to produce a probable temperature measurement uncertainty of ±91 degrees Kelvin or ±3.6% for a nominal temperature of 2600 K.

5.2 Recommendations

Several recommendations have resulted from this work. One is that special care be taken during the calibration procedure and that the procedures be studied to determine more accurately the amount of spatial bias uncertainty resulting from it. The numbers used for the precision indices of the calibration constants are possibly incorrect for two reasons. The first reason is the small number of samples used to define them. The second reason is that perhaps the procedure was carried out with more care than is generally taken during actual calibrations. A further study needs to be made which would determine if the results arrived upon in this work are correct in relation to the precision indices of the calibration constants. Fortunately, it would require an increase by a factor of 100 in the precision index of these paramters to cause a noticeable change in the uncertainty in the temperature. Therefore it seems unlikely that the values reported here are off by a sufficient amount as to significantly affect the temperature uncertainty. Nevertheless a further study is recommended to prove this.

A second recommendation, and the most important one, is that further work be done to determine the precision index in the emissivity more accurately. By far the most influential parameter in equation 15 is the emissivity precision uncertainty. It is very important to point out that the precision index of the emissivity amounts to almost 98% of the uncertainty in the temperature. A very large value was assumed for the emissivity precision index because it was actually unknown and simple analysis of the flow conditions indicate that the value chosen, 0.1, includes all anticipated values of the emissivity. An in depth study of the emissivity variations at the nozzle throat based on influences of the various species present, the fluid mechanics of the flow, and combustor effects is necessary to determine the emissivity uncertainty and its distribution acros the flow in the throat with greater accuracy.

A third recommendation is that very careful alignment procedures be followed in installing the luminosity probes. Such care is necessary to prevent bias errors in the spatial resolution from being significant.

Until additional work is done on this problem it is recommended that when analyzing temperature profiles obtained in the CFFF flowtrain using the new modified probe, the value of ±91 K be used with confidence as a value for the relative temperature measurement uncertainty.

LIST OF REFERENCES

LIST OF REFERENCES

1. Galanga, F. L., Lineberry, J. T., Wu, Y. C. L., Scott, M. H., Baucum, W. E., and Clemons, R. W., "Experimental Results of the UTSI Coal-Fired MHD Generator and Investigations of Various Power Take-Off Schemes," University of Tennessee Space Institute, AIAA 19th Aerospace Sciences Meeting, 1981.

2. Kowalik, R. M. and Kruger, C. H., "Preliminary Experiments Concerning Inhomogeneities in Combustion MHD Generators," Proceedings of the 17th Symposium on Engineering Aspects of Magnetohydrodynamics, 1978.

3. Vasil'eva, I. A., "Determining the Nonuniform Plasma Temperature Using a Generalized Line Reversal Method," Journal of Applied Spectroscopy, Vol. 22, p. 203, 1975.

4. Abernathy, R. B., "Handbook, Uncertainty in Gas Turbine Measurements," Technical Report AEDC-TR-73-5, Arnold Engineering Development Center, 1973.

5. Sparrow, E. M. and Cess, R. D., Radiation Heat Transfer, Brooks/Cole Publishing Company, Belmont, California, pp. 3-9, 1966.

6. Beyer, W. H., CRC Standard Math Tables, CRC Press, Inc., Boca Raton, Florida, 25th Edition, p. 386, 1981.

7. Winkleman, B. C., Giel, T. V., Jr. and Baucum, W. E., "Temperature and Spectral Emission/Transmission Measurements in the DOE Coal-Fired Flow Facility," Proceedings of the 21st Symposium on Engineering Aspects of MHD, 1983.

8. Hwang, C. J., "A Theoretical Study of Compressible Two Phase Internal Flow," Doctoral Dissertaion, The University of Tennessee Space Institute, DOE Report DOE/ET/10815-99, 1984.

9. Grum, F. and Becherer, R. J., Optical Radiation Measurements, Academic Press, New York, New York, Vol. 1, pp. 221-222, 1979.

VITA

Jeffrey A. Evans was born on December 1, 1960 in Columbia, South Carolina. He graduated from Thomson High School, Thomson, Georgia, in June 1978. The following September he entered the Georgia Institute of Technology, and in June 1982 he received a Bachelor of Science degree in Applied Physics.

In August 1982 the author married the former Marissa Garcia de Paredes of Panama, Republic of Panama.

In September of 1982 he accepted a research assistantship at the University of Tennessee Space Institute and began study toward a Master's degree. Following the completion of his Master's degree he plans to take a position with Control Laser Corporation of Orlando, Florida.